3D printed diffractive optical elements for rapid prototyping

Fan, Daniel; Smith, Carlas S.; Unnithan, Ranjith R.; Kim, Sejeong

Important note
To cite this publication, please use the final published version (if applicable).
Please check the document version above.

3D printed diffractive optical elements for rapid prototyping

Daniel Fan [a],[*], Carlas S. Smith [b], Ranjith R. Unnithan [a], Sejeong Kim [a]

[a] Department of Electrical and Electronic Engineering, Faculty of Engineering and Information Technology, University of Melbourne, Parkville, VIC 3010, Australia
[b] Delft Center for Systems and Control, Faculty of Mechanical Engineering, Delft University of Technology, Mekelweg 2, Delft 2628CD, the Netherlands

ARTICLE INFO

ABSTRACT

A rapid and robust method to fabricate transmission diffractive optical elements in the visible wavelengths is presented. By additive manufacturing of a polymeric photo-resin using 2-photon lithography followed by encasing of the structure in another resin with similar refractive index, the height of the structure can be made much larger, thus trading-off fabrication height for refractive index difference of the two materials. After adjusting for resin shrinkage, different diffractive optical element designs including an m = 1 vortex plate, and Laguerre-Gaussian beams with azimuthal and radial indices of (1,1), (1,2), and (2,1) were demonstrated. Experimental results show intensity patterns matching that of simulations, including size and features, although some aberration was observed, possibly due to fabrication tolerance errors or beam misalignment. This technique adds to the toolkit of micro-optics fabrication methods using additive manufacturing and 3D printing, and it would be beneficial for rapid prototyping and integration with miniaturised systems.

1. Introduction

Diffractive optical elements (DOEs) modify the phase of an incoming light beam's wavefront to produce a structured light beam. These light beams have found a wide variety of application ranging from optical tweezing [1], communications systems [2], augmented reality and sensing [3], point-spread-function engineering for microscopy [4], etc. Traditional manufacturing of DOEs such as via glass grinding and polishing, micromachining, nanoimprint lithography, grey-scale lithography, and multiple rounds of lithographic patterning and etching can be tedious or require costly tooling [5–7], and is limited to 2.5D non-free-form structures on standardised substrates, while reflective type adaptive optics using deformable mirrors or spatial light modulators for wavefront shaping requires bulky and expensive equipment.

Recent progress in additive manufacturing of optics and micro-optics has made fabrication and rapid prototyping of custom optics designs widely available and cost-effective. 2-photon lithography (2PL) in particular has allowed manufacturing of polymer-based optics with high accuracy and simplicity [8]. Optical grade smooth surfaces can be accomplished by post-processing [9] or dose control [10]. Free-form inorganic micro-lenses have been fabricated via direct write lithography and high temperature annealing, however, design dependent structural shrinkage must be considered [11]. Control over the local refractive index via laser dependent degree of polymerisation has

allowed 4D printing of graded index optical elements [12–14]. Further, direct write additive manufacturing methods has permitted fabrication of compound micro-lenses on non-standard substrates such as the end of optical fibres [2,15,16]. Besides 2PL, lower resolution stereolithography [17] and inkjet printing [18] based fabrication of optical elements such as lenses has also been achieved, albeit with lower optical quality or the need for extensive post-processing and process optimisation [19].

For the fabrication of DOEs, which requires precise modification of wavefront phase, fabrication tolerances can be particularly stringent [20]. Not only the surface roughness but also the absolute structure heights must be precise to impart the correct phase change. However, by immersing a polymer structure in another medium with similar refractive index, the fabrication tolerances can be loosened as it is traded-off for precision in the refractive index. This technique has been shown in the fabrication of DOEs by liquid immersion [21] as well as resin immersion using a moulding process [4].

In this work, we adapt this concept to direct write additive manufacturing using 2PL for the first time, which has the benefit of trading-off the fabrication height tolerance and the material refractive index value tolerance, allowing a more robust process compared to 2PL alone [22] or relying on exact refractive index differences [13,21]. The novel method presented here improves on the lateral resolution of additively manufactured DOEs reported using multi-resin stereo-lithography (SLA) [4], providing access to DOEs with ~0.2 μm lateral

---

* Corresponding author.
  E-mail address: fan.d@unimelb.edu.au (D. Fan).

resolution (an improvement of ~100× vs. SLA). By choosing different immersion resins, the height of the DOE can also be optimised, ranging from a few microns to hundreds of microns, depending on the refractive index difference. This allows process optimisation and trade-off between phase resolution, resin shrinkage effects, total height of the optical element, and process tolerances. 2PL fabricated DOEs can thus be much thinner than SLA/moulded DOEs by ~1–2 orders of magnitude, suiting applications which require flat optics, such as point-spread-function engineering in microscopy where thinner phase plates result in decreased field dependencies [23].

The equivalent phase resolution that can be accessed using resin immersion combined with 2PL is also much higher than using a single resin alone for DOE fabrication. For example, although fibre-tip orbital angular momentum generators have been reported using single-step additive manufacturing [16,22], multi-material DOEs allows improved phase resolution and superior trade-offs between fabrication tolerances. Single-step 2PL of a m = 1 vortex plate had a reported height resolution of 50 nm, equivalent to ~π/13 phase steps at 632.8 nm operating wavelength [22]. Using resin immersion as presented in this work, the phase resolution would be ~π/158, i.e., ~10 times higher. Further, 2PL allows the fabrication of DOEs on non-standard substrates such as optical fibres, microfluidic channels, and curved surfaces, and allows integration of DOEs into existing device structures [24].

2. Theory and calculations

For a DOE, the incoming wavefront is typically collimated, and it is designed for a particular operating wavelength. As the light wave passes through a transmissive material, its phase will be retarded according to

Fig. 1. a) A DOE fabricated from a single material operating in air modifies the wavefront of an input light source. b) A DOE fabricated from two materials allows trade-off between refractive index difference and fabrication height to perform the same wavefront shaping. c) The 2π height of a DOE vs. refractive index difference at various operating wavelengths, plotted in log-log scale. Region i) requires precise height fabrication while region ii) requires precise control over refractive index difference. The dotted region is explored in this work.

the refractive index difference and height variation of the material (Fig. 1a). To impart a phase shift of $\Delta\phi$ radians, the height of the material must therefore be varied according to the equation:

$$\Delta\phi = \frac{2\pi h}{\lambda}(n_1 - n_2) \tag{1}$$

where λ is the operating wavelength, h is the height of the material, and n_1 and n_2 are the refractive indices of the two different mediums the light passes through [21]. For example, for a glass DOE ($n_1 = 1.5$) in air ($n_2 = 1$) to impart a phase difference of 2π, the DOE must have a height of 2λ (Fig. 1a). By combining two materials with different refractive indices such that front and back interfaces with air are flat and parallel, the height of the DOE structure can be adjusted according to the refractive index difference, allowing larger DOE structures with looser fabrication tolerances (Fig. 1b). This can also be seen by considering the total wavefront phase error [21] using error propagation, where $\Delta n = n_1 - n_2$:

$$\delta\Delta\phi = \frac{2\pi}{\lambda} \bullet \Delta n \bullet \delta h + \frac{2\pi}{\lambda} \bullet h \bullet \delta n \tag{2}$$

and the symbol δ indicates error in that variable. In the case of a glass DOE in air, the height of the element is ~2λ (i.e., ~1 μm for optical wavelengths), while Δn is relatively large meaning that δh must be kept small to minimise the phase error (Eq. 2, first term). Furthermore, depending on the different phase shifts required throughout the DOE, the height resolution of the element must be increased to control multiple phase shift levels. Therefore, the fabrication tolerance of height profiles over different regions of the DOE is stringent. For the glass DOE in air with phase shifts in the range of 0 to 2π, height precision in fabrication needs to be in the order of tens of nm (Fig. 1c, region i). This is commonly achieved through precision micromachining such as glass grinding and polishing or multiple rounds of lithography and etching. Such methods can be both expensive and time-consuming, making them unsuitable for cost-effective rapid prototyping.

Conversely, multi-material DOEs using near-refractive-index matching [4,21] can be fabricated using stereolithography and light-projection based 3D printing of resin masters and moulding of the DOE [4]. By choosing Δn to be <<0.1, fabrication heights accessible by standard table-top 3D resin printers can be realised (Fig. 1c, region ii). However, given the large height, the error in δn can propagate as a large phase error (Eq. 2, second term), and this method is thus sensitive to small changes in refractive index. Changes in refractive index can occur due to humidity, temperature, and environmental changes, as well as degree of curing, resin aging, and mechanical stress. For example, it has been shown that the degree of polymerisation as controlled by the laser writing power affects the refractive index of a directly written 4D structure [12–14], where there is an uncertainty in the exact refractive index of the material. Dose fluctuations during the fabrication process can thus introduce a small error in δn. Further, 4D printing requires the whole volume to be written, while the resin immersion method presented here can be adapted for moulding processes which are much faster.

Additive manufacturing using 2PL allows fabrication of 3D structures with <1 μm height resolution. This allows a trade-off between high precision manufacturing of 3D structures and high precision control over the refractive index of multi-materials. By operating in an intermediate region (Fig. 1c, circled region), tolerances in both fabrication height and refractive index value can be balanced and traded-off, and errors in either will not significantly affect the phase error of the DOE. Further, 2PL has the advantage of being able to fabricate micro-optical elements, for example, at the ends of optical fibres or within microfluidic channels. In this work we evaluate the use of 2PL combined with refractive index matching with a second material to fabricate DOEs quickly, suitable for rapid prototyping.

3. Material and methods

Simulation of DOEs to be tested was performed using the scalar diffraction Python package "diffractio" [25]. A 594 nm beam with collimated Gaussian profile (FWHM ≈ 5 mm) passing through a 1.5 mm diameter DOE and then a f = 150 mm lens is propagated using the Rayleigh-Sommerfeld approximation. The intensity is calculated at the focal plane, reflecting the physical experimental arrangement. For process optimisation, a spiral phase plate producing a vortex beam with m = 1 topological charge was designed, simulated, fabricated, and characterised. For further demonstrations, Laguerre-Gaussian beams with azimuthal and radial indices of (1, 1), (1, 2), and (2, 1) respectively were designed, fabricated, and evaluated. The DOE designs produced in simulation were saved as bitmap images to be uploaded to the direct write laser fabrication tool as height maps (Fig. 2a), with heights calculated as per eq. 1 and according to the refractive indices of the resins used (Table 1) [26,27]. Bitmap resolution was matched to the resolution of the writing tool. Python scripts used for the simulation of DOE light propagation for a variety of beams and production of the height map images for fabrication are supplied in the supplementary material.

Fabrication of DOEs was performed by first preparing fused silica or ITO coated substrates (Nanoscribe GmbH, Karlsruhe, Germany) with propan-2-ol (IPA) (VLSI, RCI Labscan, Thailand) rinse and O_2 plasma treatment for 30 s (Piezobrush PZ3, relyon plasma GmbH, Germany) for promoting surface adhesion. The first structure was then direct laser

written (Fig. 2b, i) using 2PL (Photonic Professional GT2, Nanoscribe GmbH, Karlsruhe, Germany) with a variety of standard writing parameters and configurations as listed in Table 1, at nominal full laser power of 50 mW at 780 nm wavelength. The written structure was then developed for 25 min in propylene glycol monomethyl ether acetate (PGMEA) (ReagentPlus >99.5%, Sigma-Aldrich, U.S.A.) followed by 5 min in IPA and then blow-dried with N_2 air gun. A precision 80 μm thick stainless-steel shim (W0127-FP-016-0008-S2, Small Parts and Bearings Pty Ltd., Australia) used as a spacer was placed around the written structure (Fig. 2b, ii) and then a droplet of the second resin was drop-cast onto this structure (Fig. 2b, iii). A #1.5 thick (~130–170 μm thick), 20 mm × 20 mm large glass coverslip (Sail Brand, China) rinsed with IPA and dried with N_2 air gun was then carefully placed on top of the droplet and shim using tweezers to avoid air bubbles. The sandwiched structure was then taped onto the bottom of a flat falcon dish so that substrate, shim, and coverslip are in contact and parallel with each other. The assembly was then placed under a metal-halide UV curing lamp (14.67 mW/cm^2 at 405 nm, Dymax 2000-EC, U.S.A.) for 15 min and then under direct sunlight for several days to fully cure the thick second resin (Fig. 2b, iv). The completed assembly was then placed in a 3D printed holder (PLA material, Mk4 filament printer, Prusa Research, Czech Republic) and securely glued together.

Characterisation of the fabricated DOEs was performed as follows: an optical microscope (Nikon Eclipse LV150, Japan) was used to inspect the quality of the fabricated DOEs during each of the fabrication steps. Height measurements were performed using an optical profilometer (Contour GT-I, Bruker, U.S.A.) to calculate resin shrinkage after development (Fig. 2d). To characterise their function, light from a fibre-coupled laser with 594 nm wavelength (OBIS, Coherent Corp., U.S.A.) was collimated and expanded to ~5 mm diameter using a 10× objective (UIS2 PLN, Olympus, Japan). The beam was filtered through a 594 nm long-pass filter and then steered onto the fabricated DOE via an adjustable iris. The transmitted light then passed through a f = 150 mm lens onto a CMOS camera (2.2 μm pixel size, 2592 × 1944-pixel resolution, YW500, ShenZhen YangWang Technology Co Ltd., China) resulting in an intensity image (Fig. 2c). Interferograms were also imaged by using two 50:50 half-silvered mirrors and two silver mirrors in the Mach-Zehnder configuration with the DOE in one arm of the interferometer, with the combined beams imaged onto the CMOS camera without any lens (Fig. 2c). The beams were steered to be off axis to clearly show the interference fringes.

4. Results

To evaluate the concept, a 1.5 mm diameter vortex phase plate with m = 1 topological charge was designed and fabricated. Simulations show a 200 μm diameter doughnut shaped intensity pattern is expected, with the middle dark spot due to phase discontinuities in the middle of the vortex plate. Several different resin and writing combinations were tried (Table 1). 2PL writing of the first resin using IP-S and 25× objective resulted in DOE surfaces with large amounts of roughness and stitching lines. After encasing with a variety of second resins (Table 1), these DOEs were evaluated by passing collimated 594 nm wavelength laser light through them and imaging on a CMOS camera via a lens. However, no doughnut shaped intensity images were formed, only scattered light patterns, indicating that the DOE was not functioning as designed, possibly due to the roughness of the 2PL written surface profile. In this case, 25× "Solid" (hatch distance = 0.5 μm, slice distance = 1 μm, laser power = 100% or 50 mW, scan speed = 100 mm/s) recipe was used.

On the other hand, 2PL writing of the first resin using IP-Dip2 and 63× objective, and then encasing with IP-S as the second resin (giving Δn = 0.041 [26,27]) and curing under a UV lamp, resulted in formation of doughnut shaped intensity patterns as per the designed m = 1 vortex DOE. Optical inspection after the first fabrication step showed modest roughness and stitching lines (Fig. 2e), while after encasing in the second resin much of the roughness was smoothed (Fig. 2f). In this case,
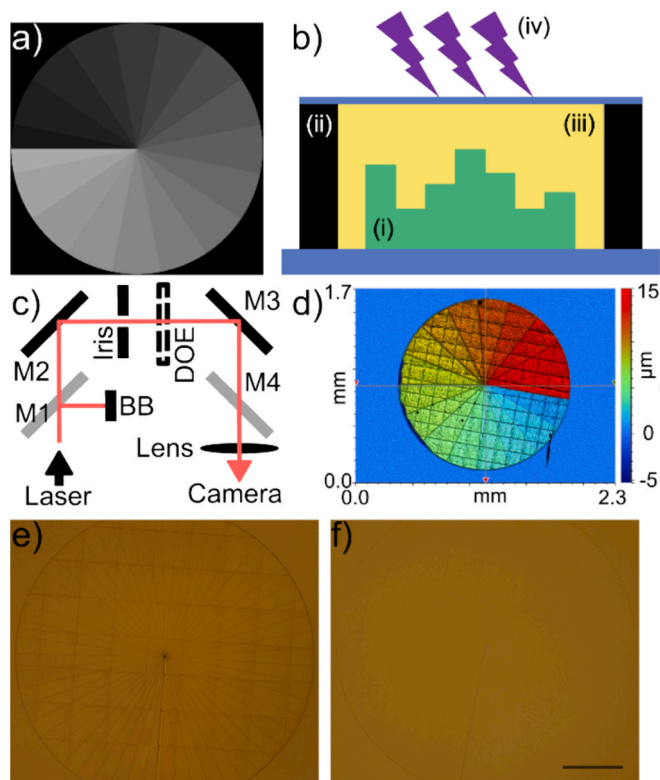
Fig. 2. a) A heightmap of a m = 1 vortex phase plate converted from amount of required phase change to height using Eq. 1. b) Fabrication procedure used in this work where i) a calculated heightmap is manufactured using 2-photon lithography, ii) a precision spacer is placed around it, iii) a second resin with matched refractive index is drop-cast on top and the assembly sealed with a glass coverslip, and iv) curing the second resin using UV light. c) Measurement setup for intensity measurement and off-axis holography where M1 and M4 are 50:50 beam-splitters. For off-axis holography the beam-block (BB) and lens are removed. d) Example optical profilometry measurement of m = 1 vortex plate showing fabricated DOE height. e) m = 1 vortex plate in optical microscope before and f) after encasing in second resin. Scale bar is 200 μm for e) and f).

Table 1

Different resins, 2PL recipes, refractive index differences, and summary of results attempted in this work. Writing time (third column) is for a 1.5 mm diameter DOE with specified height (eighth column).

Resin 1 (2PL)	Obj./Recipe	Time	n_1 [26]	Resin 2 (UV)	n_2 [27]	Δn	2π height	Result
IP-S	25× "Solid"	~0.2 h	1.515	IP-Dip2	1.547	−0.032	18.6 µm	Scattered beam
IP-S	25× "Solid"	~0.6 h	1.515	IP-S	1.506	0.009	66 µm	Scattered beam
IP-Dip2	63× "Solid"	~8.5 h	1.547	IP-S	1.506	0.041	14.5 µm	Vortex observed
IP-Dip2	63× "Swift"	~0.8 h	1.547	IP-S	1.506	0.041	14.5 µm	Vortex observed
IP-Dip2	25× "Solid"	~0.2 h	1.547	IP-S	1.506	0.041	14.5 µm	Scattered beam

63× "Solid" (hatch distance = 0.2 µm, slice distance = 0.3 µm, laser power = 40% or 20 mW, scan speed = 10 mm/s) and 63× "Swift" (hatch distance = 0.35 µm, slice distance = 0.9 µm, laser power = 95% or 47.5 mW, scan speed = 25 mm/s) recipes were used.

Optical profilometry showed that the DOE heights after the first fabrication step were slightly lower than that of the designed DOE height map (Fig. 2d). These minor height discrepancies were possibly due to resin shrinkage. To quantify the amount of shrinkage, m = 1 vortex plates with different 0 to 2π heights were designed, fabricated, and measured using optical profilometry. Designed height differences of 14.4, 15.1, 15.9, 16.6, 17.3, and 18 µm were fabricated and measured to result in actual height differences of 13.5 (−6.8%), 14.2 (−6%), 15 (−4.2%), 15.5 (−6.3%), 16.5 (−4%), and 17.5 µm (−2.3%) respectively (value in brackets being the shrinkage in percent). The average amount of shrinkage was 4.9% although it is noted that as the structures became taller the amount of height shrinkage lessened. Thus, we took the shrinkage at the target height of ~14.5 µm for future shrinkage adjustments (i.e., ~6% shrinkage was used for all further DOEs).

Next, the intensity pattern of the doughnuts produced by the m = 1 vortex plates with different 0 to 2π heights were inspected qualitatively (Fig. 3a). In the figure, the percentage value indicates the difference in 2π height between the fabricated vortex plate and the calculated design height (for 594 nm input and Δn = 0.041, resulting in a 2π height of 14.5 µm). Vortex plates with heights different from the design height clearly show side-lobes in the doughnut intensity pattern, while the vortex plate that is closest in height to the design height (second from left, −1.8% difference), shows the most symmetric doughnut intensity pattern and is thus closest to the expected simulation intensity pattern. This indicates that the assumption of Δn = 0.041 is fairly accurate.

We also varied the input laser intensity for the vortex plate closest to design height (Fig. 3a, second from left), with the doughnut intensity pattern clearly discernible from low to high intensity (Fig. 3b). The central intensity minimum was clearly observable for very high intensities such that the camera was saturated at its fastest exposure setting (Fig. 3b, furthest right).

Using the measured shrinkage amount (~6%), we then designed,

simulated, fabricated, and evaluated more complex DOEs. Besides the m = 1 vortex plate (Fig. 4a), Laguerre-Gaussian beams with azimuthal and radial indices of (1, 1) (Fig. 4b), (1, 2) (Fig. 4c), and (2, 1) (Fig. 4d)
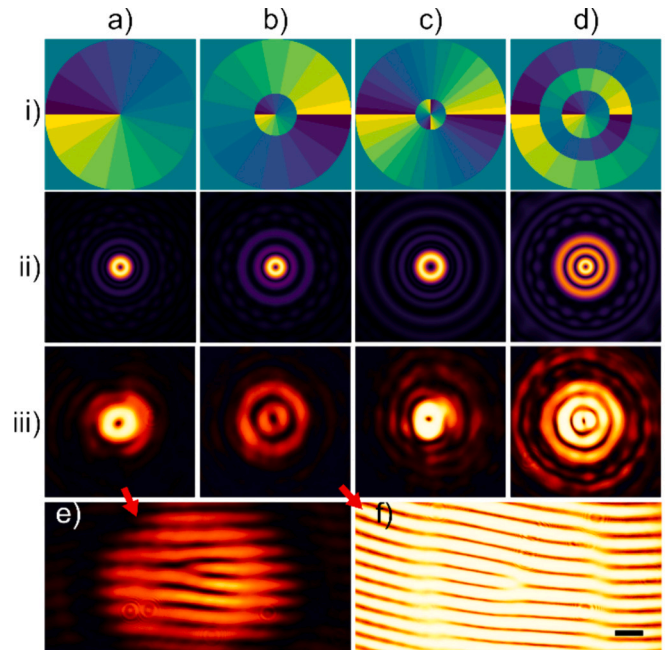
Fig. 4. The i) calculated phase profile, ii) simulated intensity pattern, and iii) experimental intensity pattern of various DOEs with 1.5 mm diameter. a) m = 1 vortex phase plate. b) Laguerre-Gaussian (azimuthal index = 1, radial index = 1). c) Laguerre-Gaussian (azimuthal index = 1, radial index = 2). d) Laguerre-Gaussian (azimuthal index = 2, radial index = 1). e) Interferogram of m = 1 vortex plate using off-axis holography. f) Interferogram of Laguerre-Gaussian (azimuthal index = 1, radial index = 1) beam. Scale bar for all intensity images (ii), (iii), (e), and (f) is shown on the bottom right and equals 200 µm.
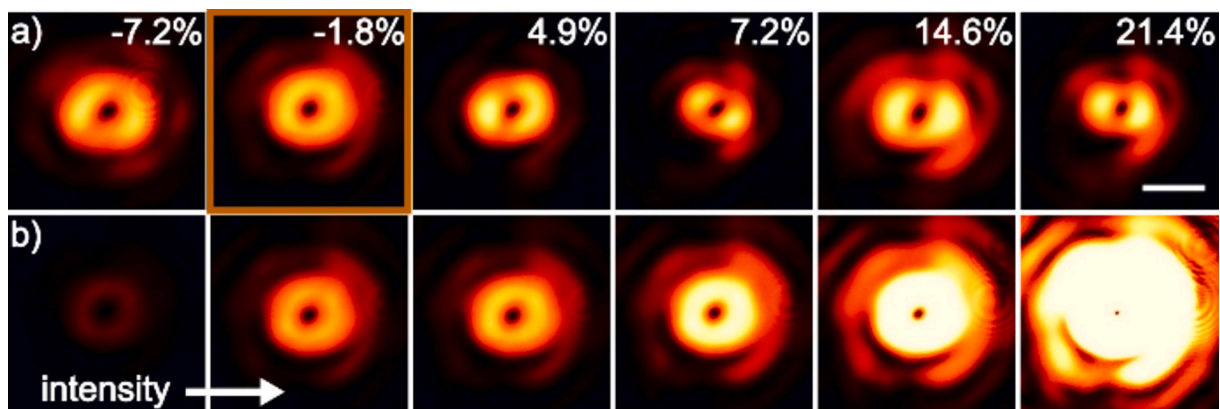
Fig. 3. a) Intensity patterns of light beam passing through a m = 1 vortex phase plate with different heights (indicated by the percentage value difference compared with 14.5 µm height) and imaged on camera via a f = 150 mm lens. b) The second from left (in a, highlighted) phase plate used at increasing intensity showing a clear central minimum even at high laser intensities. Scale bar for all intensity patterns (far right) equals 200 µm.

respectively, with 1.5 mm diameter were characterised. Fig. 4i) shows the phase pattern for each type of DOE, calculated from the provided Python script (see supplementary material) while Fig. 4ii) shows the simulated intensity pattern for the four types of DOEs, and Fig. 4iii) shows the experimentally measured intensity pattern on camera. The measured intensity patterns match simulations well, both in shape, features, and dimensions. Nevertheless, some aberrations in the features were apparent, such as the shape of the secondary intensity rings. This could be due to misalignment of the setup, shape of the cut-off iris, or fabrication tolerance errors. The errors include presence of stitching lines, surface roughness, or structure tilt where each writing field is tilted slightly due to overall substrate tilt and the fact that the interface position is recalibrated for each writing field. Further investigation is required to isolate the source of aberrations.

Finally, interferograms of the DOEs were recorded using off-axis holography by removing the tube lens and introducing a reference light arm via beam-splitters (Fig. 2c). The interferogram for the m = 1 vortex plate (Fig. 4e) clearly shows a fork in the centre, indicating a topological charge of 1 and wrapping of phase. The interferogram for the Laguerre-Gaussian (1, 1) DOE (Fig. 4f) not only shows the fork in the centre of the DOE but also in the 1st azimuthal ring the phase can be clearly seen to shift (from far left of the image in Fig. 4f to the far right of the image), showing the phase profile of both the 0th azimuthal zone and the 1st azimuthal zone.

5. Discussion

Results show that after considering resin shrinkage, DOE fabrication was straightforward, and the structured light produced by the DOE under experiment matched the expected simulated intensity pattern qualitatively in terms of intensity features and size. However, aberrations were observed across all tested DOEs. This might be related to small errors in the optical alignment and the shape of the cut-off iris. Note that the iris was placed a few centimetres away from the DOE and stray diffracted light might illuminate unwanted sections of the DOE assembly such as outside the printed structure. It would be advised to place the iris as close as possible to the DOE, or even better, directly print optically opaque irises next to the DOE to cut-off any stray light [28]. In addition, the size of the iris was adjusted by hand, and thus the DOE illumination in the experiment may not exactly match that of the phase profile used in simulation. This can cause slight differences in the size of intensity patterns for simulation vs. experiment (Fig. 4).

Further, shrinkage values varied according to different structure dimensions, and thus a small amount of process optimisation is required to tune to the correct shrinkage values to achieve the correct structure heights. Once optimised, shrinkage was observed to be fairly consistent across half a dozen DOE samples, although care must be taken during processing to ensure consistency. Since the DOEs presented here are flat with one dimension much smaller than the other dimensions, shrinkage is also consistent across the DOE. This might not be the case for more complex DOEs with different and more complicated geometries, where resin shrinkage effects must be optimised.

Optical inspection and profilometry of the print quality showed a reasonable surface roughness. Tool specifications for the small feature solution set (i.e., 63× objective "swift", Table 1) indicate a roughness <20 nm, which for near-index matching where $\Delta n \sim 0.04$, corresponds to an effective roughness <1 nm. However, for the medium feature solution set (i.e., 25× objective "solid", Table 1), no beams were formed, possibly due to the large hatching and slicing distances of this writing recipe that causes roughness and large lateral features. This might be mitigated in future by optimization of the writing process, for example by decreasing the hatching distance and thus increasing overlap between lines, a smoother surface can be achieved using the larger spot size of the 25× objective to improve writing speed as well as roughness. The maximum lateral resolution of the Nanoscribe GT2 tool is specified at 0.2 μm, thus limiting DOE designs in the in-plane directions. This can

possibly be addressed by using post-processing to improve final structure resolution [29]. The minimum lateral resolution shown in this work to still achieve formed DOE beams was the 0.35 μm slicing distance used in the 63× "Swift" recipe.

Further, stitching lines were obviously present between writing fields, and these regions might exhibit much larger discrepancies which can also cause aberrations in the DOE produced intensity pattern. Latest developments in 2PL technology have reduced stitching to be much smaller and future 2PL fabrication is expected to produce very low surface roughness with minimal field stitching [30]. Precise measurement of the refractive indices of different cured resins is also necessary for full process optimisation.

Another source of aberrations might be the assembly process where the second resin is drop-cast, and a coverslip is placed on top. Pressure is made via Kapton tape to hold the surfaces flat during curing but too much pressure might cause distortions in the glass surfaces. The UV curing process itself may cause stresses in the resin, especially if too much dose is applied too quickly. As such it might be advisable to cure the second resin slowly, or to use resins that can be cured by other means. Another option is in-situ multi-material 3D printing with a specialty head that can exchange different resins [31]. In this way both resins are 2PL cured and fabrication is more robust. A third option is to use 2PL written structures as mould masters, similar to [4] but with looser refractive index tolerances. This technique is therefore suited to mass-production in roll-to-roll processes for example, which is more difficult to accomplish with SLA/resin-matching based DOEs [4] as fabrication height for SLA is much taller. Autofluorescence arising from the photo-resin [26] might also be avoided by using moulding processes, which could be important depending on the application. Aberrations may also appear over time due to resin aging, environmental effects, or mechanical effects, which can all affect the refractive index difference between the two resins. On the other hand, since resins have different wavelength dependent refractive indices, via careful resin selection, broadband DOEs might be realised.

In summary, a process for rapid prototyping of DOEs using direct write 2PL combined with immersion in another resin with similar refractive index was demonstrated. For simple structured light such as vortex beams, the produced intensity patterns showed the expected features for a variety of intensities, albeit with slight aberrations possibly due to misalignments in the optical system. The rapid prototyping of DOEs is particularly useful in the evaluation of wavefront shaping elements used in microscopy such as point-spread-function engineering [4] and multi-focal imaging [32] and would also find a variety of applications in astronomy, remote sensing, communications, etc. One advantage of using additive manufacturing for DOE fabrication over moulding is the ability to fabricate DOEs on non-standard substrates such as curved surfaces (e.g., glasses for augmented reality), at the end facets of optical fibres [15], and integrated within more complicated microfluidic devices [33]. Such micro-DOEs would allow beam shaping in confined spaces such as in microfluidic cytometry, medical endoscopy, and photonic systems-on-chip. In combination with microfluidics, such DOEs would allow adaptive control over the wavefront, for example by exchanging liquids with different refractive indices, resulting in transmission adaptive optical elements. Together with recent developments in additive manufacturing of complex micro-optical systems with smooth optical curvatures [30], printing of opaque light stops [28], laser-induced refractive index variations for graded index lenses [12,13], etc., multi-material rapid prototyping of DOEs offers another technique in the arsenal of wavefront shaping and optics fabrication using 3D printing.

Declaration of competing interest

The authors declare that they have no known competing financial interests or personal relationships that could have appeared to influence the work reported in this paper.

Data availability

Data will be made available on request.

Acknowledgements

Appendix A. Supplementary data

Supplementary data to this article can be found online at https://doi.org/10.1016/j.mne.2024.100270.

References

[1] E. Otte, C. Denz, Optical trapping gets structure: structured light for advanced optical manipulation, Appl. Phys. Rev. 7 (2020) 041308, https://doi.org/10.1063/5.0013276.

[2] C. Li, T. Wieduwilt, F.J. Wendisch, A. Márquez, L. de S. Menezes, S.A. Maier, M. A. Schmidt, H. Ren, Metafiber transforming arbitrarily structured light, Nat. Commun. 14 (2023) 7222, https://doi.org/10.1038/s41467-023-43068-7.

[3] Y. Ni, S. Chen, Y. Wang, Q. Tan, S. Xiao, Y. Yang, Metasurface for structured light projection over 120° field of view, Nano Lett. 20 (2020) 6719–6724, https://doi.org/10.1021/acs.nanolett.0c02586.

[4] R. Orange Kedem, N. Opatovski, D. Xiao, B. Ferdman, O. Alalouf, S. Kumar Pal, Z. Wang, H. von der Emde, M. Weber, S.J. Sahl, A. Ponjavic, A. Arie, S.W. Hell, Y. Shechtman, Near index matching enables solid diffractive optical element fabrication via additive manufacturing, Light Sci. Appl. 12 (2023) 222, https://doi.org/10.1038/s41377-023-01277-1.

[5] M.R. Taghizadeh, P. Blair, B. Layet, I.M. Barton, A.J. Waddie, N. Ross, Design and fabrication of diffractive optical elements, Microelectron. Eng. 34 (1997) 219–242, https://doi.org/10.1016/S0167-9317(97)00188-3.

[6] A.G. Poleshchuk, V.P. Korolkov, V.P. Veiko, R.A. Zakoldaev, M.M. Sergeev, Laser Technologies in Micro-Optics. Part 2. Fabrication of elements with a three-dimensional profile, Optoelectron. Instrum. Data Process. 54 (2018) 113–126, https://doi.org/10.3103/S8756699018020012.

[7] V. Garg, R.G. Mote, J. Fu, Rapid prototyping of highly ordered subwavelength silicon nanostructures with enhanced light trapping, Opt. Mater. 94 (2019) 75–85, https://doi.org/10.1016/j.optmat.2019.05.020.

[8] D. Gonzalez-Hernandez, S. Varapnickas, A. Bertoncini, C. Liberale, M. Malinauskas, Micro-optics 3D printed via multi-photon laser lithography, Adv. Opt. Mater. 11 (2023) 2201701, https://doi.org/10.1002/adom.202201701.

[9] N. Chidambaram, R. Kirchner, R. Fallica, L. Yu, M. Altana, H. Schift, Selective surface smoothening of polymer microlenses by depth confined softening, Adv. Mater. Technol. 2 (2017) 1700018, https://doi.org/10.1002/admt.201700018.

[10] T. Aderneuer, O. Fernández, R. Ferrini, Two-photon grayscale lithography for free-form micro-optical arrays, Opt. Express 29 (2021) 39511, https://doi.org/10.1364/OE.440251.

[11] D. Gonzalez-Hernandez, S. Varapnickas, G. Merkininkaitė, A. Čiburys, D. Gailevičius, S. Šakirzanovas, S. Juodkazis, M. Malinauskas, Laser 3D printing of inorganic free-form Micro-optics, Photonics 8 (2021) 577, https://doi.org/10.3390/photonics8120577.

[12] X. Porte, N.U. Dinc, J. Moughames, G. Panusa, C. Juliano, M. Kadic, C. Moser, D. Brunner, D. Psaltis, Direct (3+1)D laser writing of graded-index optical elements, Optica 8 (2021) 1281, https://doi.org/10.1364/OPTICA.433475.

[13] C.R. Ocier, C.A. Richards, D.A. Bacon-Brown, Q. Ding, R. Kumar, T.J. Garcia, J. van de Groep, J.-H. Song, A.J. Cyphersmith, A. Rhode, A.N. Perry, A.J. Littlefield, J. Zhu, D. Xie, H. Gao, J.F. Messinger, M.L. Brongersma, K.C. Toussaint, L. L. Goddard, P.V. Braun, Direct laser writing of volumetric gradient index lenses and waveguides, Light Sci. Appl. 9 (2020) 196, https://doi.org/10.1038/s41377-020-00431-3.

[14] D. Gonzalez-Hernandez, B. Sanchez-Padilla, D. Gailevičius, S.C. Thodika, S. Juodkazis, E. Brasselet, M. Malinauskas, Single-step 3D printing of Micro-optics with adjustable refractive index by ultrafast laser nanolithography, Adv. Opt. Mater. 11 (2023) 2300258, https://doi.org/10.1002/adom.202300258.

[15] I.V.A.K. Reddy, A. Bertoncini, C. Liberale, 3D-printed fiber-based zeroth- and high-order Bessel beam generator, Optica 9 (2022) 645, https://doi.org/10.1364/OPTICA.453839.

[16] A. Žukauskas, Improvement of the fabrication accuracy of Fiber tip microoptical components via mode field expansion, J. Laser MicroNanoeng. 9 (2014) 68–72, https://doi.org/10.2961/jlmn.2014.01.0014.

[17] X. Chen, W. Liu, B. Dong, J. Lee, H.O.T. Ware, H.F. Zhang, C. Sun, High-speed 3D printing of millimeter-size customized aspheric imaging lenses with sub 7 nm surface roughness, Adv. Mater. 30 (2018) 1705683, https://doi.org/10.1002/adma.201705683.

[18] B.G. Assefa, M. Pekkarinen, H. Partanen, J. Biskop, J. Turunen, J. Saarinen, Imaging-quality 3D-printed centimeter-scale lens, Opt. Express 27 (2019) 12630, https://doi.org/10.1364/OE.27.012630.

[19] T. Blachowicz, G. Ehrmann, A. Ehrmann, Optical elements from 3D printed polymers, E-Polym. 21 (2021) 549–565, https://doi.org/10.1515/epoly-2021-0061.

[20] H. Wang, H. Wang, W. Zhang, J.K.W. Yang, Toward near-perfect diffractive optical elements *via* nanoscale 3D printing, ACS Nano 14 (2020) 10452–10461, https://doi.org/10.1021/acsnano.0c04313.

[21] R. Orange-Kedem, E. Nehme, L.E. Weiss, B. Ferdman, O. Alalouf, N. Opatovski, Y. Shechtman, 3D printable diffractive optical elements by liquid immersion, Nat. Commun. 12 (2021) 3067, https://doi.org/10.1038/s41467-021-23279-6.

[22] H. Wei, A.K. Amrithanath, S. Krishnaswamy, 3D printing of Micro-optic spiral phase plates for the generation of optical Vortex beams, IEEE Photon. Technol. Lett. 31 (2019) 599–602, https://doi.org/10.1109/LPT.2019.2903151.

[23] M. Siemons, C.N. Hulleman, R.Ø. Thorsen, C.S. Smith, S. Stallinga, High precision wavefront control in point spread function engineering for single emitter localization, Opt. Express 26 (2018) 8397, https://doi.org/10.1364/OE.26.008397.

[24] P. Erfle, J. Riewe, H. Bunjes, A. Dietzel, Goodbye fouling: a unique coaxial lamination mixer (CLM) enabled by two-photon polymerization for the stable production of monodisperse drug carrier nanoparticles, Lab Chip 21 (2021) 2178–2193, https://doi.org/10.1039/D1LC00047K.

[25] L.M. Sanchez Brea, Diffractio, python Module for Diffraction and Interference Optics. https://pypi.org/project/diffractio/, 2019.

[26] Nanoscribe, Nanoguide, (n.d.). https://support.nanoscribe.com (accessed February 22, 2024).

[27] T. Gissibl, S. Wagner, J. Sykora, M. Schmid, H. Giessen, Refractive index measurements of photo-resists for three-dimensional direct laser writing, Opt. Mater. Express 7 (2017) 2293, https://doi.org/10.1364/OME.7.002293.

[28] M.D. Schmid, A. Toulouse, S. Thiele, S. Mangold, A.M. Herkommer, H. Giessen, 3D direct laser writing of highly absorptive photoresist for miniature optical apertures, Adv. Funct. Mater. 33 (2023) 2211159, https://doi.org/10.1002/adfm.202211159.

[29] G. Seniutinas, A. Weber, C. Padeste, I. Sakellari, M. Farsari, C. David, Beyond 100 nm resolution in 3D laser lithography — post processing solutions, Microelectron. Eng. 191 (2018) 25–31, https://doi.org/10.1016/j.mee.2018.01.018.

[30] L. Siegle, S. Ristok, H. Giessen, Complex aspherical singlet and doublet microoptics by grayscale 3D printing, Opt. Express 31 (2023) 4179, https://doi.org/10.1364/OE.480472.

[31] Heteromerge, Functional 3D Micro-Printing, (n.d.). https://www.heteromerge.com (accessed February 22, 2024).

[32] S. Abrahamsson, J. Chen, B. Hajj, S. Stallinga, A.Y. Katsov, J. Wisniewski, G. Mizuguchi, P. Soule, F. Mueller, C.D. Darzacq, X. Darzacq, C. Wu, C. I. Bargmann, D.A. Agard, M. Dahan, M.G.L. Gustafsson, Fast multicolor 3D imaging using aberration-corrected multifocus microscopy, Nat. Methods 10 (2013) 60–63, https://doi.org/10.1038/nmeth.2277.

[33] E.J. Vargas-Ordaz, S. Gorelick, H.M. York, B. Liu, M.L. Halls, S. Arumugam, A. Neild, A. de Marco, V.J. Cadarso, Three-dimensional imaging on a chip using optofluidics light-sheet fluorescence microscopy, Lab Chip 21 (2021) 2945–2954, https://doi.org/10.1039/D1LC00098E.